First Measurement of the Charged Current Cross Section at HERA

H1 Collaboration

Abstract:

The cross section of the charged current process $e^- p \rightarrow \nu_e + hadrons$ is measured at HERA for transverse momenta of the hadron system larger than $25\,\text{GeV}$. The size of the cross section exhibits the W propagator.

H1 Collaboration

T. Ahmed[3], V. Andreev[24], B. Andrieu[27], R.-D. Appuhn[11], M. Arpagaus[34], A. Babaev[25], J. Bán[17], P. Baranov[24], E. Barrelet[28], W. Bartel[11], M. Barth[4], U. Bassler[28], H.P. Beck[35], H.-J. Behrend[11], A. Belousov[24], Ch. Berger[1], H. Bergstein[1], G. Bernardi[28], R. Bernet[34], G. Bertrand-Coremans[4], M. Besançon[9], P. Biddulph[22], J.C. Bizot[26], V. Blobel[13], K. Borras[8], V. Boudry[27], A. Braemer[14], F. Brasse[11], W. Braunschweig[1], V. Brisson[26], D. Bruncko[17], C. Brune[15], L. Büngener[13], J. Bürger[11], F.W. Büsser[13], A. Buniatian[11,37], S. Burke[18], G. Buschhorn[25], A.J. Campbell[11], T. Carli[25], F. Charles[28], D. Clarke[5], A.B. Clegg[18], M. Colombo[8], J.A. Coughlan[5], A. Courau[26], Ch. Coutures[9], G. Cozzika[9], L. Criegee[11], D.G. Cussans[5], J. Cvach[27], S. Dagoret[28], J.B. Dainton[19], M. Danilov[23], A.W.E. Dann[22], W.D. Dau[16], K. Daum[32], M. David[9], E. Deffur[11], B. Delcourt[26], L. Del Buono[28], A. De Roeck[11], E. De Wolf[4], C. Dollfus[35], J.D. Dowell[3], H.B. Dreis[2], J. Duboc[28], D. Düllmann[13], O. Dünger[13], H. Duhm[12], J. Ebert[32], T.R. Ebert[19], G. Eckerlin[11], V. Efremenko[23], S. Egli[35], H. Ehrlichmann[33], S. Eichenberger[35], R. Eichler[34], F. Eisele[14], E. Eisenhandler[20], R.J. Ellison[22], E. Elsen[11], M. Erdmann[14], E. Evrard[4], L. Favart[4], A. Fedotov[23], D. Feeken[13], R. Felst[11], J. Feltesse[9], J. Ferencei[15], F. Ferrarotto[31], K. Flamm[11], W. Flauger[11,†], M. Fleischer[11], M. Flieser[25], G. Flügge[2], A. Fomenko[24], B. Fominykh[23], M. Forbush[7], J. Formánek[30], J.M. Foster[22], G. Franke[11], E. Fretwurst[12], E. Gabathuler[19], K. Gamerdinger[25], J. Garvey[3], J. Gayler[11], M. Gebauer[8], A. Gellrich[13], H. Genzel[1], R. Gerhards[11], U. Goerlach[11], L. Goerlich[6], N. Gogitidze[24], M. Goldberg[28], D. Goldner[8], A.M. Goodall[19], I. Gorelov[23], P. Goritchev[23], C. Grab[34], H. Grässler[2], R. Grässler[2], T. Greenshaw[19], G. Grindhammer[25], C. Gruber[16], J. Haack[33], D. Haidt[11], L. Hajduk[6], O. Hamon[28], E.M. Hanlon[18], M. Hapke[11], W.J. Haynes[5], J. Heatherington[20], V. Hedberg[21], G. Heinzelmann[13], R.C.W. Henderson[18], H. Henschel[33], R. Herma[1], I. Herynek[29], W. Hildesheim[11], P. Hill[5], C.D. Hilton[22], J. Hladký[29], K.C. Hoeger[22], M. Höppner[8], Ph. Huet[4], H. Hufnagel[14], M. Ibbotson[22], H. Itterbeck[1], M.-A. Jabiol[9], A. Jacholkowska[26], C. Jacobsson[21], M. Jaffre[26], J. Janoth[15], T. Jansen[11], L. Jönsson[21], K. Johannsen[13], D.P. Johnson[4], L. Johnson[18], H. Jung[2], P.I.P. Kalmus[20], S. Kazarian[11], R. Kaschowitz[2], P. Kasselmann[12], U. Kathage[16], H.H. Kaufmann[33], I.R. Kenyon[3], S. Kermiche[26], C. Keuker[1], C. Kiesling[25], M. Klein[33], C. Kleinwort[13], G. Knies[11], W. Ko[7], T. Köhler[1], H. Kolanoski[8], F. Kole[7], S.D. Kolya[22], V. Korbel[11], M. Korn[8], P. Kostka[33], S.K. Kotelnikov[24], M.W. Krasny[6,28], H. Krehbiel[11], D. Krücker[2], U. Krüger[11], M. Krüner-Marquis[11], J.P. Kubenka[25], H. Küster[2], M. Kuhlen[25], T. Kurča[17], J. Kurzhöfer[8], B. Kuznik[32], D. Lacour[28], F. Lamarche[27], R. Lander[7], M.P.J. Landon[20], W. Lange[33], P. Lanius[25], J.F. Laporte[9], A. Lebedev[24], C. Leverenz[11], S. Levonian[11,24], Ch. Ley[2], A. Lindner[8], G. Lindström[12], F. Linsel[11], J. Lipinski[13], P. Loch[26], H. Lohmander[21], G.C. Lopez[20], D. Lüers[25,†], D. Lüke[8,11], N. Magnussen[32], E. Malinovski[24], S. Mani[7], P. Marage[4], R. Marshall[22], J. Martens[32], R. Martin[19], H.-U. Martyn[1], J. Martyniak[6], S. Masson[2], A. Mavroidis[20], S.J. Maxfield[19], S.J. McMahon[19], A. Mehta[22], K. Meier[15], D. Mercer[22], T. Merz[11], C.A. Meyer[35], H. Meyer[32], J. Meyer[11], V. Milone[31], D. Milstead[19], F. Moreau[27], J.V. Morris[5], G. Müller[11], K. Müller[35], P. Murín[17], V. Nagovizin[23], B. Naroska[13], Th. Naumann[33], G. Nawrath[8], P.R. Newman[3], D. Newton[18], D. Neyret[28], H.K. Nguyen[28], F. Niebergall[13], C. Niebuhr[11], R. Nisius[1], G. Nowak[6], G.W. Noyes[3], M. Nyberg-Werther[21], H. Oberlack[25], U. Obrock[8], J.E. Olsson[11], A. Panitch[4], C. Pascaud[26], G.D. Patel[19], E. Peppel[11], E. Perez[9], J.P. Phillips[22], Ch. Pichler[12], W. Pilgram[2], D. Pitzl[34], G. Pope[7], S. Prell[11], R. Prosi[11], G. Rädel[11], F. Raupach[1], P. Reimer[29], S. Reinshagen[11], P. Ribarics[25], V. Riech[12], J. Riedlberger[34], S. Riess[13], M. Rietz[2], S.M. Robertson[3], P. Robmann[35], R. Roosen[4], A. Rostovtsev[23], C. Royon[9], M. Ruffer[12], S. Rusakov[24], K. Rybicki[6], N. Sahlmann[2], E. Sanchez[25], D.P.C. Sankey[5], M. Savitsky[23], P. Schacht[25], P. Schleper[14], W. von Schlippe[20], C. Schmidt[11], D. Schmidt[32], A. Schöning[11], V. Schröder[11], M. Schulz[11], B. Schwab[14], A. Schwind[33], U. Seehausen[13], F. Sefkow[11], R. Sell[11], A. Semenov[23], V. Shekelyan[23], I. Sheviakov[24], H. Shooshtari[25], L.N. Shtarkov[24], G. Siegmon[16], U. Siewert[16],

Y. Sirois[27], I.O. Skillicorn[10], P. Smirnov[24], J.R. Smith[7], Y. Soloviev[24], H. Spitzer[13],
P. Staroba[29], M. Steenbock[13], P. Steffen[11], R. Steinberg[2], B. Stella[31], K. Stephens[22], J. Stier[11],
J. Stiewe[15], U. Stösslein[33], J. Strachota[29], U. Straumann[35], W. Struczinski[2], J.P. Sutton[3],
S. Tapprogge[15], R.E. Taylor[36,26], V. Tchernyshov[23], C. Thiebaux[27], G. Thompson[20],
I. Tichomirov[23], P. Truöl[35], J. Turnau[6], J. Tutas[14], A. Usik[24], S. Valkar[30], A. Valkarova[30],
C. Vallée[28], P. Van Esch[4], P. Van Mechelen[4], A. Vartapetian[11,37], Y. Vazdik[24], M. Vecko[29],
P. Verrecchia[9], G. Villet[9], K. Wacker[8], A. Wagener[2], I.W. Walker[18], A. Walther[8], G. Weber[13],
D. Wegener[8], A. Wegner[11], H. P.Wellisch[25], L.R. West[3], S. Willard[7], M. Winde[33],
G.-G. Winter[11], Th. Wolff[34], A.E. Wright[22], E. Wünsch[11], N. Wulff[11], T.P. Yiou[28], J. Žáček[30],
Z. Zhang[26], M. Zimmer[11], W. Zimmermann[11], F. Zomer[26], and K. Zuber[15]

[1] *I. Physikalisches Institut der RWTH, Aachen, Germany[a]*
[2] *III. Physikalisches Institut der RWTH, Aachen, Germany[a]*
[3] *School of Physics and Space Research, University of Birmingham, Birmingham, UK[b]*
[4] *Inter-University Institute for High Energies ULB-VUB, Brussels, Belgium[c]*
[5] *Rutherford Appleton Laboratory, Chilton, Didcot, UK[b]*
[6] *Institute for Nuclear Physics, Cracow, Poland[d]*
[7] *Physics Department and IIRPA, University of California, Davis, California, USA[e]*
[8] *Institut für Physik, Universität Dortmund, Dortmund, Germany[a]*
[9] *DAPNIA, Centre d'Etudes de Saclay, Gif-sur-Yvette, France*
[10] *Department of Physics and Astronomy, University of Glasgow, Glasgow, UK[b]*
[11] *DESY, Hamburg, Germany[a]*
[12] *I. Institut für Experimentalphysik, Universität Hamburg, Hamburg, Germany[a]*
[13] *II. Institut für Experimentalphysik, Universität Hamburg, Hamburg, Germany[a]*
[14] *Physikalisches Institut, Universität Heidelberg, Heidelberg, Germany[a]*
[15] *Institut für Hochenergiephysik, Universität Heidelberg, Heidelberg, Germany[a]*
[16] *Institut für Reine und Angewandte Kernphysik, Universität Kiel, Kiel, Germany[a]*
[17] *Institute of Experimental Physics, Slovak Academy of Sciences, Košice, Slovak Republik*
[18] *School of Physics and Materials, University of Lancaster, Lancaster, UK[b]*
[19] *Department of Physics, University of Liverpool, Liverpool, UK[b]*
[20] *Queen Mary and Westfield College, London, UK[b]*
[21] *Physics Department, University of Lund, Lund, Sweden[f]*
[22] *Physics Department, University of Manchester, Manchester, UK[b]*
[23] *Institute for Theoretical and Experimental Physics, Moscow, Russia*
[24] *Lebedev Physical Institute, Moscow, Russia*
[25] *Max-Planck-Institut für Physik, München, Germany[a]*
[26] *LAL, Université de Paris-Sud, IN2P3-CNRS, Orsay, France*
[27] *LPNHE, Ecole Polytechnique, IN2P3-CNRS, Palaiseau, France*
[28] *LPNHE, Universités Paris VI and VII, IN2P3-CNRS, Paris, France*
[29] *Institute of Physics, Czech Academy of Sciences, Praha, Czech Republik*
[30] *Nuclear Center, Charles University, Praha, Czech Republik*
[31] *INFN Roma and Dipartimento di Fisica, Universita "La Sapienza", Roma, Italy*
[32] *Fachbereich Physik, Bergische Universität Gesamthochschule Wuppertal, Wuppertal, Germany[a]*
[33] *DESY, Institut für Hochenergiephysik, Zeuthen, Germany[a]*
[34] *Institut für Mittelenergiephysik, ETH, Zürich, Switzerland[g]*
[35] *Physik-Institut der Universität Zürich, Zürich, Switzerland[g]*
[36] *Stanford Linear Accelerator Center, Stanford California, USA*
[37] *Visitor from Yerevan Phys.Inst., Armenia*
[†] *Deceased*

1 Introduction

The weak charged current was extensively investigated during the accelerator neutrino physics era [1]. In the early sixties the driving idea was the search for the massive intermediate vector boson ($W^{\pm}$) thought to be responsible for weak interactions. The linear increase of the total neutrino cross section with energy should be damped due to the W propagator. From the compatibility with linearity, lower limits on the W mass could be derived. Initial values of a few GeV were gradually increased to about 20 GeV as higher energy proton synchrotrons allowed the construction of higher energy neutrino beams. Following the discovery of weak neutral currents, electromagnetic and weak phenomena could be unified in a single *electroweak* framework. In it, the W mass is related to the electroweak mixing parameter $\sin^2 \Theta_W$ via α/G, the known ratio of the fine structure and the Fermi constants. The W mass could thus be predicted. From the early measurements of $\sin^2 \Theta_W$ it became obvious that M_W would not be accessible in neutrino experiments (see fig. 1).

The *ep*-collider HERA extends the investigation of weak interactions by exploring, for the first time, the reaction $e^- p \rightarrow \nu_e + hadrons$ in a high energy kinematic region in which the W propagator plays a prominent role. The reaction is the inverse of neutrino-nucleon scattering, where the electron energy corresponds to an equivalent 50 TeV beam energy in a fixed target experiment. The W propagator enters in the differential cross section with the term $1/(1 + Q^2/M_W^2)^2$. The measurement of the total cross section at HERA implies an integration over Q^2 ranging up to about 10^5 GeV^2. Consequently, $< Q^2 >$ is now comparable to $M_W^2 = (80\,\text{GeV})^2$ causing a substantial deviation from the linear behaviour observed at low energies. The luminosity collected by the H1 experiment during 1993 provides a sufficiently large charged current event sample to exhibit the W propagator effect.

2 Method

Charged current events at large values of the 4-momentum transfer squared, Q^2, provide a clear signature, namely an unbalanced high transverse momentum hadron system due to the undetected final state neutrino. This discriminates efficiently against other processes, such as neutral current and γp events, which are approximately balanced. From the momenta of the final state hadrons, two observables can be computed [2], the *scalar* (S) and *vector* (V) transverse momentum sums:

$$S \equiv \sum_i |\vec{p}_{\perp i}|$$

$$V \equiv |\sum_i \vec{p}_{\perp i}| .$$

S and V are closely related to the total transverse energy and the missing transverse energy in each event. They are straightforward to compute, requiring only the calorimeter cell energies
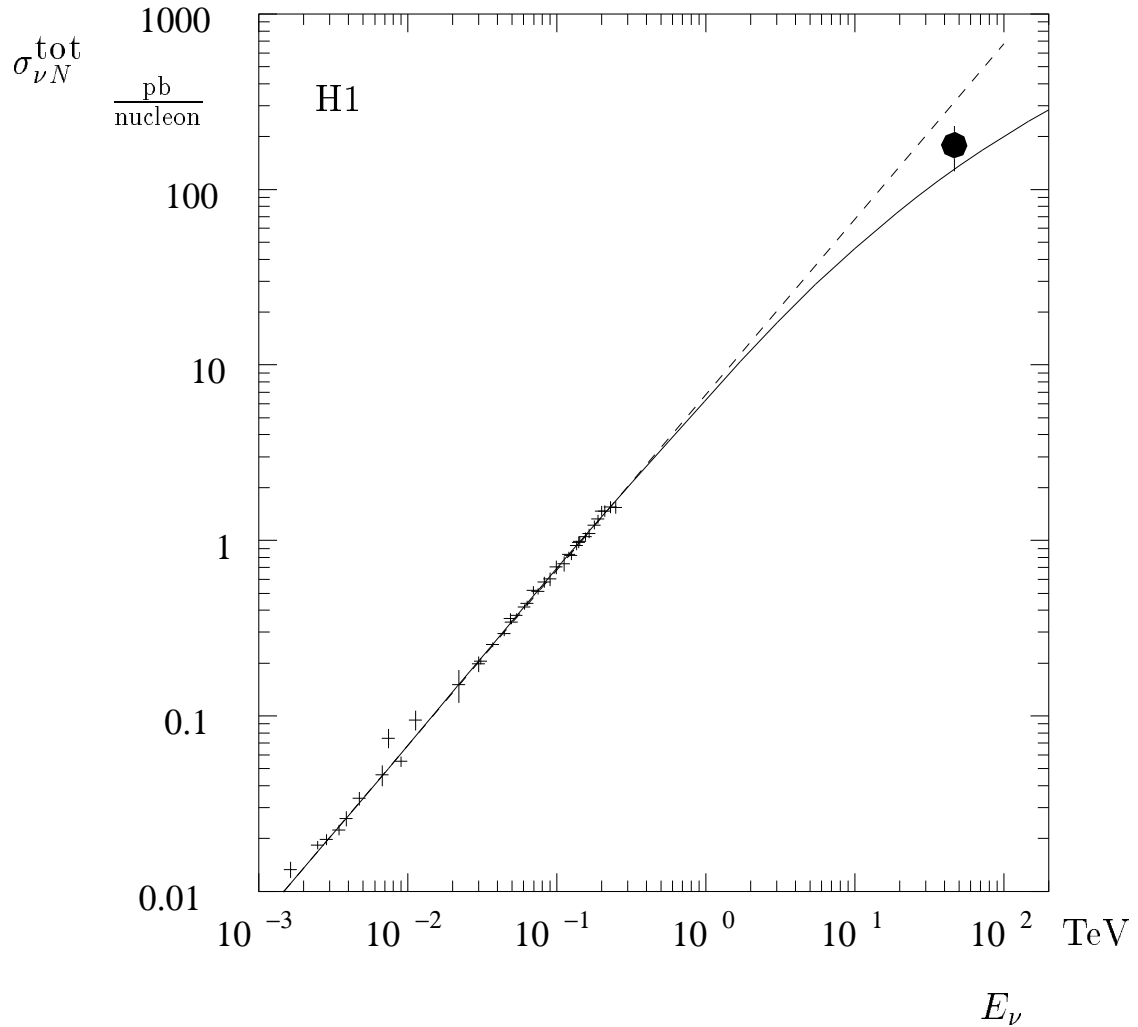
Figure 1: *The energy dependence of the νN cross section. The crosses represent the low energy neutrino data (see ref. [1], p. 213) while the full circle refers to the result of this analysis which, for the purpose of comparison, has been converted to a νN cross section. The experiment at HERA corresponds to an equivalent fixed target energy of about 50 TeV. The full line represents the predicted cross section including the W propagator. The dashed line is the linear extrapolation from low energies.*

and positions and the event vertex position. Charged current events are characterized by large values of S and V. Note that by definition $S \geq V$. The main selection criterion for charged current candidates is based on the observable V. The choice of the cut $V > 25\,\mathrm{GeV}$ appears to be a reasonable compromise between background rejection and statistics. The large value of V implies $Q^2 > 625$ GeV^2 and thus emphasizes the importance of the W propagator term. Furthermore, events in the kinematic region defined by $V > 25\,\mathrm{GeV}$ do not suffer from large radiative effects.

Neutral current events constitute an ideal control sample. Once the scattered electron is discarded, their topology is similar to charged current events. The available statistics for events then satisfying $V > 25\,\mathrm{GeV}$ is about 10 times larger than for the charged current sample owing to the contribution of the photon propagator.

3   Experimental Conditions

This analysis is based on data taken in 1993. The beam energies were 26.7 GeV for electrons and 820 GeV for protons. HERA was operated with 94 electron and 90 proton bunches filled out of the 220 possible bunches separated by 96 ns. 84 bunches were in collision. 10 electron and 6 proton bunches had no collision partner. The length of the interaction region is determined by the proton bunch length and extends over a region of width $\sigma = 10$ cm along the beam line. Each event is associated with a particular bunch number.

A detailed description of the H1 detector and its performance can be found in [3]. Only those aspects with relevance for the measurement of the total charged current cross section are discussed below.

The energy of the hadronic final state is measured in the highly segmented liquid argon (LAr) calorimeter [4], which covers a polar angular range between 4° and 153° with respect to the proton beam direction. It consists of an electromagnetic section with lead absorber and a hadronic section with stainless steel absorber. The total depth of the electromagnetic part varies between 20 and 30 radiation lengths, whereas the total depth of both calorimeters combined varies between 4.5 and 8 interaction lengths. The calibration of the LAr calorimeter segments has been obtained from test beam measurements using electrons and pions [3, 4, 5]. The energy calibration for the electromagnetic section is known to an overall accuracy of 3% as determined from a comparison of the measured track momentum of electrons and positrons with the corresponding energy deposition in the calorimetric cells in the H1 detector. The hadronic energy is calibrated to 5% as determined from studies of the transverse momentum balance in deep inelastic scattering events. Charged particles are measured in the central jet drift chamber (CJC) of polar angular acceptance $15° - 165°$ and are used to determine an event vertex. The time of occurrence of each event is determined from tracks which cross the CJC sense wire planes and produce a prompt signal with a precision of 1.5 ns.

The hardware trigger for charged current events ("CC trigger") consists of two conditions:

- The vector sum of transverse momenta, evaluated at the first trigger level using a coarsely segmented calorimeter trigger readout, has to exceed a threshold set just above the noise and well below the physics requirement of 25 GeV.

- The time of the event has to be given by a fast track trigger, which requires hits in at least 3 out of 4 proportional chamber layers. This trigger restricts the vertex coordinate along the beam direction to about ± 40 cm.

This trigger is well adapted to the topology of CC events. Note that the two independent conditions can also be fulfilled by an accidental superposition of two unrelated events.

The luminosity is measured using the rate of small angle Bremsstrahlung [3]. The electron and the photon are detected in crystal calorimeters positioned at $33\,\mathrm{m}$ and $103\,\mathrm{m}$, respectively, from the interaction point along the direction of the incident e beam direction.

4   The Event Sample

The main selection criterion for charged current candidates requires a cut in the momentum imbalance:

$$V > 25\,\mathrm{GeV}.$$

In addition, the following selection criteria are imposed:

- The CC trigger is fulfilled.

- A vertex is reconstructed.

- The event passes the halo and cosmic muon filters. Residual superimposed events are removed in a visual scan.

14 events satisfy these criteria.

The background processes to be considered fall into two categories, beam related processes and those induced by incoming muons.

Background from incoming Muons

Incoming muons from cosmic rays or beam halo may induce large and localized showers in the LAr calorimeter, which are not momentum balanced with respect to the interaction point. The pattern created by such muons is detected in the muon detector surrounding the experiment and in the LAr calorimeter, which is sensitive to the small energy deposits of minimum ionizing particles. Due to the vertex requirement this background is considerably suppressed. Nevertheless, it may enter the event sample in two ways, namely (a) the muon induced shower emits charged particles which accidentally fulfill the vertex requirement, or (b) a muon is superimposed over a beam induced interaction (beam gas or γp) which satisfies the vertex requirement.

The cosmic muon filters which are applied search for patterns compatible with penetrating muons. Their performance can be monitored by inspecting the time of the event (t_{event}). For cosmic events, the time of passage is not correlated with the time of the beam interaction (t_{ia}) which is seen in fig. 2 as a flat background appearing also in empty bunches. After applying the cosmic muon filter the remaining background from pure cosmic muons is negligible (fig. 2b).

The automatic recognition of this background has to be elaborate when an interaction of a cosmic ray muon coincides with a beam induced interaction. The shower in the calorimeter may develop several bunch crossings before or after the occurrence of the vertex defining charged particle, because the length of the LAr calorimeter signals is typically $1\,\mu\mathrm{sec}$, which is long compared to the bunch crossing interval of $96\,\mathrm{ns}$. In this case the time of the "superimposed" event is correlated with the nominal interaction time (t_{ia}). This is seen in fig. 2c where the events that have been rejected by the cosmic muon filter show a peak at the nominal interaction time. As expected, this behaviour is not seen in empty bunches.
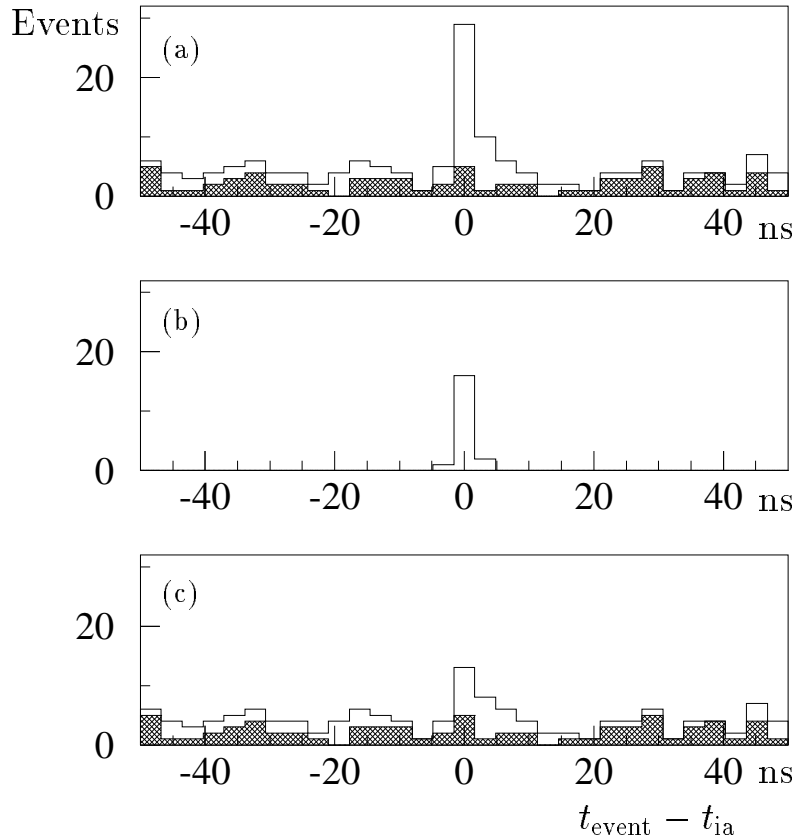
Figure 2: *The time of the selected events: (a) before (b) after applying the cosmic filters. The rejected events (c) exhibit both a flat structure from genuine cosmic rays and a small peak at 0 produced by accidental coincidences between such rays and beam interactions (superimposed events). The shaded histogram indicates the time of the events for those empty bunches where the trigger was kept active.*

Halo muons produced upstream may traverse the detector parallel to the beam line. They may generate electromagnetic showers while the track of the penetrating muon continues over the entire longitudinal range of the calorimeter at constant distance from the beam line. The signature of the halo muons is unique. The pattern of their energy deposition in the calorimeter has been searched for, and these events have been excluded from the sample. The signal of a large scintillator array placed upstream of the detector was used to verify the high efficiency of the search algorithm.

To remove residual background from superimposed events a visual scan has been performed. One halo and four cosmic muon events of this type were clearly identified and removed, giving the final sample of 14 events. The five background events had escaped the previous automatic rejection in which a conservative approach was adopted in order to retain full efficiency for CC events.

Beam related Background

Due to the large momentum imbalance required ($V > 25\,\mathrm{GeV}$) the contamination from γp, NC and beam gas events is strongly suppressed. Indeed all these beam induced background processes are balanced in momentum ($V \approx 0$), while S may assume large values. These events can simulate a CC candidate only in the case of an extreme fluctuation of the energy measurement due to either resolution or loss of particles. To the latter case belong in particular NC events with a high $p_\perp$ electron lost in the beam pipe. As these events originate from a kinematic region with very high Q^2 they contribute a negligible amount. In the region $V > 25$ GeV less than 0.1 events are expected from all these sources combined.

The 14 CC candidates are shown in the V-S plane in fig. 3, where the *signal region* is represented by the area $V > 25\,\mathrm{GeV}$. The events show the correlation between V and S expected for CC events.

A gradual decrease of the V cut would lead to a small increase of the number of CC events accompanied by the appearance of the tails of the beam related background processes. To verify this behaviour, the analysis has been extended to a region with a substantially relaxed V cut of $10\,\mathrm{GeV}$, where the detection efficiency for CC events is significantly reduced. Additional events enter predominantly at large values of S, which is indicative of the background. Indeed some of the background events identify themselves unambiguously by the presence of an isolated electron in either the small angle tagging system or the main calorimeter respectively.

In summary, the 14 CC candidates do not show any deficiencies – in particular no indication of a NC event with a badly detected electron – and are considered to be genuine CC events. A typical event is shown in fig. 4.

5   Efficiencies and Systematics

The efficiencies of the various selection steps are summarized in Table 1. The CC trigger and vertex efficiencies have been determined using a NC reference sample obtained by discarding the electron and requiring for the hadron system the same criteria as for CC candidates. This procedure works well and has been verified by a Monte Carlo simulation. The other two entries in Table 1 were evaluated using a sample of Monte Carlo [6] generated CC events.
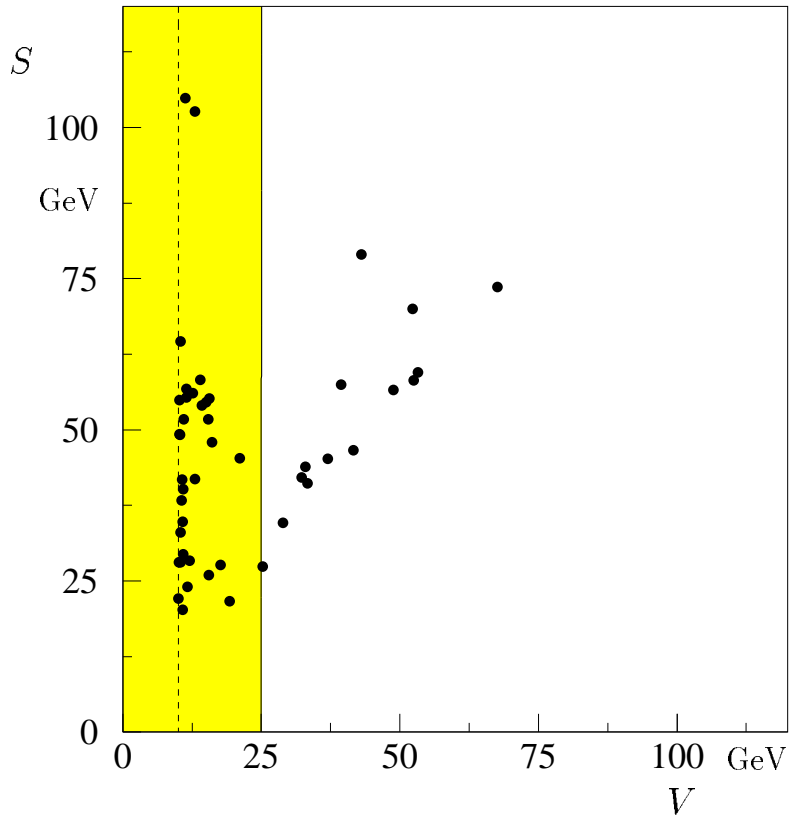
Figure 3: *Selected events in the V-S plane for V > 10 GeV. The signal region is defined by V > 25 GeV.*
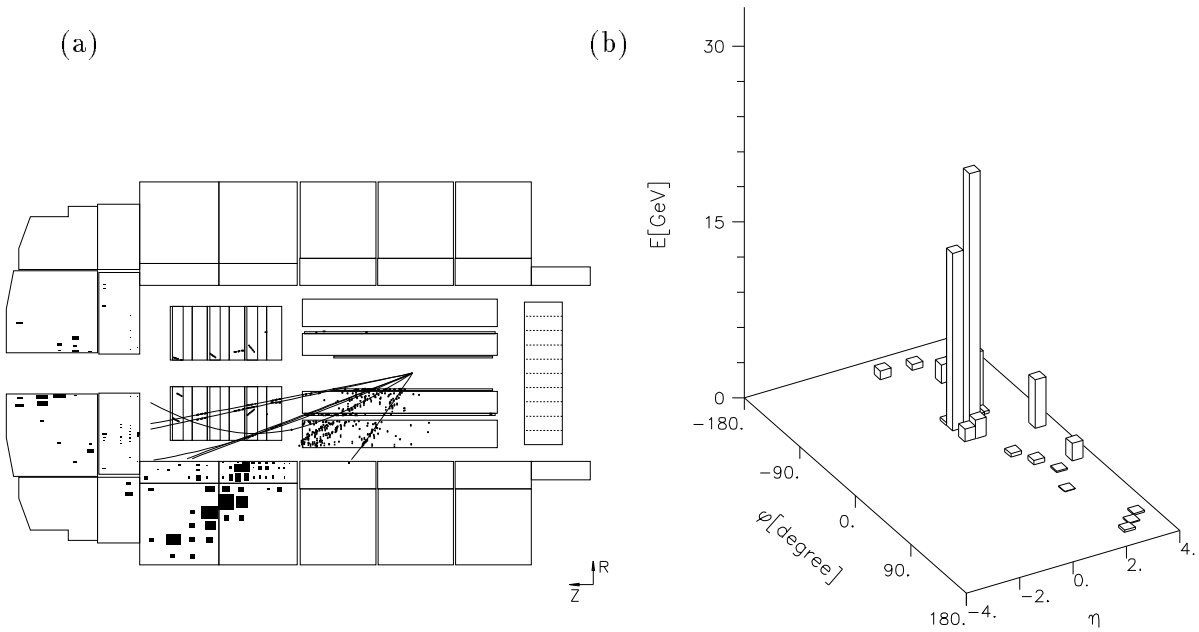

Figure 4: *A typical CC event: (a) side view of the H1 tracking system with the reconstructed tracks and the surrounding calorimeter with its energy depositions, (b) energy flow as measured in the calorimeter as a function of pseudorapidity (η) and azimuthal angle (φ).*

9

Note that the calculated efficiency for the V cut includes the effects from migration of events due to resolution, particles escaping detection. The resulting 0.97 is the sum of a gain of 3% and a loss of 6%. The requirement of a reconstructed vertex does not cause any inefficiency for hadron jets within the polar angular range which is well covered by the CJC. Those outside the angular acceptance of the CJC have a reduced probability to emit a charged particle into the jet chamber leading to an overall efficiency 0.84 ± 0.07.

selection step	efficiency
V cut	0.97 ± 0.04
CC trigger	0.92 ± 0.04
vertex	0.84 ± 0.07
cosmic muon and halo filter	0.98 ± 0.02
Total efficiency (ϵ)	0.73 ± 0.08

Table 1: *Efficiencies for the CC selection*

6   Result and Conclusion

The fully corrected charged current cross section for neutrino transverse momenta $p_\perp > 25\,\mathrm{GeV}$ is calculated as $\sigma = N/\mathcal{L}\epsilon$. The data sample used for the event selection corresponds to an integrated luminosity of $\mathcal{L} = 348 \pm 17\,\mathrm{nb}^{-1}$. The systematic error of the luminosity measurement arises predominantly from the uncertainty in the acceptance, while its statistical error is negligible. Using the above number of $N{=}14$ charged current events and the corrections given in Table 1 one obtains :

$$\sigma(p_\perp > 25\,\mathrm{GeV}) = 55 \pm 15 \pm 6\,\mathrm{pb},$$

where the first error is statistical, the second error includes all known systematic effects added in quadrature [1].

This experimental value can be compared with the theoretical expectation of 40.9 pb for $p_\perp > 25\,\mathrm{GeV}$. The calculation [7] takes into account electroweak and QCD corrections. The prediction requires knowledge of the proton structure functions, the parametrisation [8] of which is not critical, since the transverse momentum cut at 25 GeV restricts the integration domain to values in $x_{\mathrm{Bjorken}} > 0.03$ where the structure functions are well known from low energy lepton-nucleon scattering [9]. The Q^2-evolution is obtained from the Altarelli-Parisi equations which are assumed here to be valid up to the HERA energy. The uncertainty in the energy calibration is included in the systematic error of the measured cross section. If the calorimeter calibration were to be increased by 5 %, the increase in the lower limit of the integration would result in a decrease of the theoretical prediction by 1.8 pb.

Fig. 5 shows the sensitivity of the predicted cross section to the propagator mass due to presence of the term $1/(1 + Q^2/M^2_{\mathrm{prop}})^2$. The value of the propagator mass inferred from this measurement agrees well with the known resonance mass of 80.22 GeV [9] and excludes the asymptotic case (dashed line in fig. 5). With the high energy provided by the ep-collider HERA, the effect of the W propagator in deep inelastic charged current interactions is visible for the first time.

---

[1] For illustration, the measured cross section has been converted into an equivalent νN cross section to be shown in fig. 1. The conversion factor includes the extrapolation of $p_\perp$ to zero based on the parametrisation [8] and a reinterpretation as a νN cross section which takes into account the relevant flavour contributions. The extrapolation necessarily reduces the sensitivity to the propagator (cf. fig. 5).
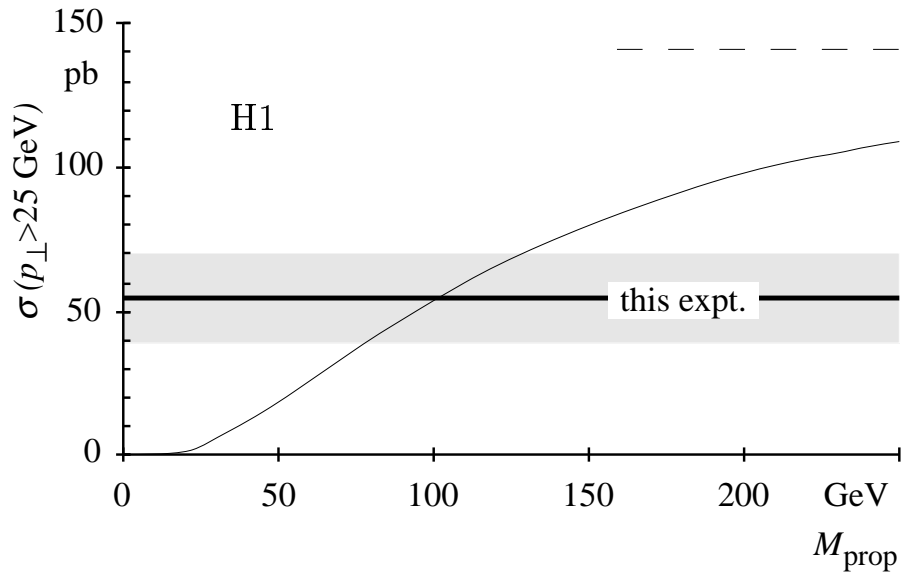
Figure 5: *The CC cross section predicted as function of the propagator mass M_{prop} (thin solid line). The dashed line indicates the asymptotic case $M_{\mathrm{prop}} = \infty$. The shaded region represents the 1σ band of the measured cross section.*

Acknowledgements

References

[1] D. Haidt and H. Pietschmann: Landolt-Börnstein New Series I/10, Springer (1988)

[2] V. Brisson et al.: *The measurement of electroweak parameters*, Proceedings of the Workshop "Physics at HERA", eds. W. Buchmüller and G. Ingelman, Hamburg, 1991, Vol. 2, 947.

[3] H1 Collab., I. Abt et al.: *The H1 detector at HERA*, DESY preprint 93-103 (1993).

[4] H1 Calorimeter Group, B. Andrieu et al.: Nucl. Instr. and Meth. **A336** (1993), 460

[5] H1 Calorimeter Group, B. Andrieu et al.: Nucl. Instr. and Meth. **A336** (1993), 499

[6] G. Ingelman: *LEPTO 6.1*, Proceedings of the Workshop "Physics at HERA", eds. W. Buchmüller and G. Ingelman, Hamburg, 1991, Vol. 3, 1366, and references therein. A. Kwiatkowski, H. Spiesberger, and H.-J. Möhring: Comp. Phys. Commun. 69 (1992) 155, and references therein.

[7] H. Spiesberger: EPRC91, unpublished program manual, 1991; Nucl.Phys. **B349** (1991) 109; *Precision Electroweak Tests at HERA*, preprint Univ. Bielefeld, BI-TP 93/03, Jan. 1993, to be publ. in *Precision Tests of the Standard Model*, Advanced Series on Directions in High Energy Physics, World Scientific Publishing Co., Ed. P. Langacker.

[8] A. Martin, R. Roberts and J. Stirling: Phys. Rev. **D47** (1993), 867; Phys. Lett. **306B** (1993), 145, Erratum **309B** (1993) 492. The parametrisation D_0' is used.

[9] Particle Data Group: Phys. Rev. **D45** (1992) II.1 and III.75.